RSC Advances

ROYAL SOCIETY OF CHEMISTRY

www.rsc.org/advances

Developing Biomedical Nano-Grained β-Type Titanium Alloys using High Pressure Torsion for Improved Cell Adherence

Hakan Yilmazer,[a,b,*] Mustafa Şen[c], Mitsuo Niinomi[b], Masaaki Nakai[b], Liu Huihong[b], Ken Cho[d], Yoshikazu Todaka[e], Hitoshi Shiku[f], and Tomokazu Matsue[f,g]

[a]Department of Metallurgical and Materials Engineering, Yildiz Technical University, Istanbul 34210, Turkey

[b]Institute for Materials Research, Tohoku University, Sendai 980-8577, Japan

[c]Department of Biomedical Engineering, Izmir Katip Celebi University, Izmir 35620, Turkey.

[d]Division of Materials and Manufacturing Science, Graduate School of Engineering, Osaka University, Osaka 565–0871, Japan

[e]Department of Mechanical Engineering, Toyohashi University of Technology, Toyohashi 441–8580, Japan

[f]Graduate School of Environmental Studies, Tohoku University, Sendai 980-8579, Japan

[g]WPI-Advanced Institute for Materials Research, Tohoku University, Sendai 980-8577, Japan

* Corresponding author.
Tel.: +90-212-383-4671
Fax: +90-212-383-4665
E-mail address: hakanyil@yildiz.edu.tr, hakan@imr.tohoku.ac.jp, yilmazerh@gmail.com

Keywords
Titanium alloys
Biomaterial
Severe plastic deformation
Orthopedic implants
Actin network structure

Abstract

Proper surface characteristic for a titanium implant is crucial for the formation of different cellular protrusions known as filopodia and lamellipodia, both of which have a significant impact on cell attachment, spreading, migration, and proliferation. Microstructural features such as grain boundaries and defects of implant surface can modulate the cellular components and structure at the leading edge of cells. Here, a nano-grained Ti-29Nb-13Ta-4.6Zr (NG TNTZ) substrate was produced by high-pressure torsion (HPT) for improved biofunctionality. Cellular response of human osteoblast cells on nano-grained TNTZ substrates is evaluated and compared with the cellular response of those on coarse-grained TNTZ. High wettability, which depends on high internal energy due to the nano-sized grains that are full of boundaries, interfaces, and high dislocation density, influenced the hOBs cells on NG TNTZ to form highly developed cellular protrusions. Large number of filopodia protrusions resulted in excellent cell attachment as consistent with high level of vinculin and superior cell proliferation. This study demonstrates the advantages of nanocrystalline surface modification using HPT for processing metallic biomaterials that are proper for orthopedic implants.

Introduction

Microstructural features such as grain structure, grain boundaries, and defects are key factors in influencing the majority of all characteristics of titanium as a polycrystalline material.[1] In recent years, the role of grain size in controlling surface bio-functionality has been investigated on a range of metallic biomaterials.[2,3] In the last decade, the development of ultrafine- and nano-grained (UFG/NG) materials has attracted particular attention because of improved mechanical and surface properties compared to those of conventional coarse–grained (CG) materials.[4] Severe plastic deformation (SPD) is an efficient process for extreme grain refinement, yielding UFG/NG materials.[5,6] For metallic materials, the numerous dislocations introduced by severe deformation gradually become arranged and annihilated into high-angle boundaries, resulting in an UFG/NG microstructure, both on the surface and in the body.[7] Such UFG/NG materials exhibit outstanding mechanical properties such as high strength and hardness, and good ductility.[6,8] The aim of this study is to produce a titanium implant exhibiting an excellent surface bio-functionality that favors cell attachment, spreading, and proliferation[9] in addition to outstanding mechanical properties[10] to allow long-term usage. However, although the surface bio-functionality of UFG/NG metallic biomaterials has been reported,[3,11] these materials are mostly fragmented, and the mechanisms of enhanced cellular behavior on implant have not been addressed in terms of the cell cytoskeleton.

Developing Nano-Grained β-Type Titanium Alloy. Herein, the use of a *β*- type Ti-29Nb-13Ta-4.6Zr (TNTZ) alloy[12] composed of non-toxic and non-allergenic elements is reported for the preparation of substrates bearing CG and UFG/NG microstructures via conventional processes such as solution and aging treatments and high-pressure torsion[7], which is one of the SPD processes. Compared to widely used implant material Ti-6A-4V ELI, which has a high Young's modulus (110 GPA), TNTZ exhibits a lower value (60-80 GPa) close to that of

bone (10-30 GPa), thus preventing stress shielding effects that can result in osteoporosis or poor osteointegration (also see the section for experiments in the ESI).[13] The microstructural characterizations of our materials were studied by optical microscopy (OM), scanning electron microscopy (SEM), transmission electron microscopy (TEM), and high-resolution TEM (HRTEM). Surface characteristics were studied by atomic force microscopy (AFM) and contact angle measurements. Surface wettability was determined by evaluating surface free energy (SFE) using contact angle measurement (also see the section for experiments in the ESI). The cellular activity of human osteoblast cells (hOBs) cultured on CG and UFG/NG TNTZ alloys was studied with respect to cell attachment and proliferation. The morphology of the attached hOBs were investigated using immunofluorescence (IF) microscopy, by labeling the nuclei, actin and vinculin proteins in the attached hOBs with blue, red, and green colors, respectively, using a Focal Adhesion Kit (also see the section for experiments in the ESI).

Material Characterization. Microstructural features of TNTZ have been summarized in Fig. 1. (Please see the supplementary section for the details of the microstructural characterization) The larger images to clearly understand the microstructures were added in the Supplementary. Previously reported XRD analysis (Figure S1)[14] clearly confirmed this BCC structure has showed a precipitated hexagonal closed packed (HCP) α phase following aging treatment ($TNTZ_{AT}$). Figures The OM micrograph in Figure 1a shows that the solutionized TNTZ ($TNTZ_{ST}$) possesses a single body-centered cubic (BCC) equiaxed β grains (~40 μm diameter) microstructure (Figure S2a). The SEM observation (Figure 1b) shows these α phases are homogeneously distributed in the β grains and exhibit a needle-like morphology (~750 nm × 25 nm) (Figure S2b).

The microstructure of $TNTZ_{AT}$ subjected to HPT ($TNTZ_{AHPT}$) was investigated by TEM (Topcon EM-002B, Japan) due to the limitations of OM and SEM (Figure 1c) (Figure S3a).

TEM bright field images (Figure 1c) show that $TNTZ_{AHPT}$ exhibits a microstructure consisting of elongated grains (~285 nm × 35 nm). In addition, a relatively homogeneous microstructure was revealed by a hardness distribution (Figure S5). The complete Debye rings in the SAED pattern of $TNTZ_{AHPT}$ also indicate highly polycrystalline microstructure (Figure 1c) (Figure S3a). Unfortunately, the α phases were difficult to distinguish in the conventional TEM bright field image. Furthermore, HRTEM (FEI Titan 80-300, Japan) revealed a precipitated α phase (red lines) with a circular morphology (~12 nm diameter) in the β grains (Figure 1d) (Figure 3b). In contrast, large blurred and wavy contrast variations (yellow dashed lines), which indicate strain fields, surrounding the α phases in the β matrix were also observed.[14] Furthermore, the elongated grains contain nanostructured subgrains with non-uniform morphology. In addition, the grains and subgrains of $TNTZ_{AHPT}$ surrounding large contrasting and blurred and wavy boundaries with remained dislocations remained during annihilation of arranged dislocations. Such a refining mechanism a long with the formation of such non-equilibrium boundaries,[6,15] have been previously reported[14] and are illustrated in Figure 1e (Figure S4).

Surface bio-functionality. Mirror-finish polishing was then performed to ensure identical surface topography for all substrates in order to investigate microstructural effect on surface bio-functionality. AFM (AFM, Nanocute, Seiko, Japan) topographical images of all polished substrates in a 10 μm × 10 μm scan area are shown in Figure S6 and mean roughness values are listed in Table S1. AFM analysis reveals that all substrates exhibit identical surface roughness and topography. Surface free energy (SFE) parameters for all substrates were then determined using the contact angle measurements with distilled water and further diiodomethane (DMs-401, Kyowa, Japan). Figure S7 shows the average contact angles and SFE values for all substrates using drops of distilled water. Although no statistically significant differences were observed among coarse grained substrates, $TNTZ_{AT}$ gives a

slightly smaller contact angle among CG $TNTZ_{ST}$, $TNTZ_{AT}$, and Ti64 ELI substrates with values of 53.80°±2.13°, 51.78°±2.87°, and 64.83°±2.40°, respectively. On the other hand, the water drops on $TNTZ_{AHPT}$ substrates show quite smaller contacted angle (35.15°±2.49°) than those of the CG substrates (Figure S7b).

Cell attachment and proliferation. The cellular behavior of hOBs has been quantitatively revealed attachment studies on titanium substrates (Figure 2) (please see the supplementary section for the details of the cell culture). Cell numbers were counted using a disposable hemocytometer (C-Chip, NanoEnTek Inc., USA). The number of hOBs attached to $TNTZ_{AHPT}$ was significantly higher than that on CG $TNTZ_{ST}$ and $TNTZ_{AT}$ substrates (Figure 2) after 6 h incubation. In addition, although the number of hOBs attached to the $TNTZ_{AT}$ was slightly higher than that on $TNTZ_{ST}$, no statistical difference was observed. Individual actin proteins, which are major determinants of shape, migration, and attachment of the hOBs, were then analyzed quantitatively using IF microscopy (Figure 3). The attached hOBs exhibit well-developed and dense actin stress fibers (ASFs) on $TNTZ_{AHPT}$ whereas ASFs were not observed in all hOBs attached to $TNTZ_{ST}$ and $TNTZ_{AT}$. The magnified IF micrographs (Figure 3a) show that the hOBs on titanium substrates exhibit lamellipodia and filopodia structures at their leading edges. These protrusions coexist at the protruding front of a migrating cell, with the filopodia tending to extend by the highly dense organization of actin filaments from bundles formed inside the lamellipodia. The titanium implant surface has to present an excellent surface characteristic for improved cell migration for ensuring implant-body biocompatibility in bone formation. The hOBs exhibit larger lamellipodia structures along with significantly higher numbers of filopodia structures on $TNTZ_{AHPT}$, than those of $TNTZ_{ST}$ and $TNTZ_{AT}$ (Figure 3b). The magnified IF micrographs also show that although filopodia structures are formed only at the leading edge of the hOBs attached on $TNTZ_{ST}$ and $TNTZ_{AT}$, they surround the majority of hOBs attached to $TNTZ_{AHPT}$ (Figure 3a).

Immunostaining of actin cytoskeleton. To better understand the substrate-hOBs interactions and the organization of actin filaments, vinculin proteins were also visualized by IF microscopy (Olympus IX71 inverted microscopy, Japan). (Figure S8a). IF micrographs of hOBs attached to $TNTZ_{AHPT}$ show significantly stronger vinculin signals than those on $TNTZ_{ST}$ and $TNTZ_{AT}$, which was verified by the quantitative data of the vinculin area/cell area in Figure S8b. In the case of hOB growth, cell proliferation on TNTZ and Ti64 ELI substrates following 6 d incubation was assessed and is illustrated in Figure S9. Although the number of hOBs was slightly higher on $TNTZ_{AT}$ than that on $TNTZ_{ST}$ and Ti64 ELI, no significant difference was observed. Furthermore, $TNTZ_{AHPT}$ gave the highest cell number of all substrates.

Discussion.

Since a relatively uniform surface roughness was maintained throughout our study, the observed cell-substrate interactions and their responses were directly related to factors arising from differences in microstructural features, such as dislocations. The energy stored in various dislocation configurations provide the dislocations provide the driving force for the observed recovery and recrystallization phenomena during the HPT.[16–18] Consequently, the exterior dislocations (Figures 1 and S4), which contribute the majority of stored energy in NG TNTZ, are integrated mainly into grain boundaries, cell boundaries, or complex entanglements. Therefore, the high surface energy of NG TNTZ (Figure S7) due to the large volume fraction of grain boundaries and interfaces exhibiting exterior dislocation. Reports suggest that materials possessing the same composition and surface topography, while having smaller grain diameter, exhibit higher surface energies than their CG counterparts.[19,20] Furthermore, in the case of NG TNTZ, a higher surface energy resulted in a higher wettability, which correlates with the ability of the solid surface to reduce surface tension, and thus reduce the contact angle of the liquid[21] when compared to CG TNTZ. Wei and his

coworkers[22] showed that high wettability increases the cell attachment due to high fibronectin absorption to a substrate surface. A similar result regarding hOBs was demonstrated on a graphene substrate by Shi and his coworkers.[23] Therefore, wettability is known to affect surface bio-functionality. This surface functionality is the basis for the osteointegration assessment, for the stimulation of hOB functions such as adhesion, spreading, and proliferation at the bone-implant interface.[24] Furthermore, HPT causes a high volume fraction of discontinuities related to the above-mentioned boundaries, interfaces, and junctions in the surface microstructure. These features can lead to the formation of focal adhesion points, which may help signaling among cells during cell attachment, along with migration and proliferation along the NG TNTZ.[25] Furthermore, it was reported that cytoskeleton dynamics have been implied by stimulated mechano-receptive responses in fibroblast, related to such discontinuities.[26]

Examining individual proteins linked to hOBs activity also indicated that NG TNTZ produced more promising results. One of the major structures of actin cytoskeleton, ASFs are formed by bundles of actin filaments in the cytoplasm stretching across the entire hOB length.[27,28] These ASFs play a central role in the attachment, migration and morphology of hOBs.[28] IF micrographs of the ASFs show that compared to CG TNTZs, the hOBs on the NG TNTZ exhibit enhanced outstretched morphologies with well-organized and elongated ASFs. In addition, lamellipodia and filopodia aid in actin network structure formation to define the leading edge for migrations.[27,28] In particular, filopodia is responsible for exploring the environment during motility.[29,30] Furthermore, the cytoplasmic actin-binding protein vinculin is mainly found in focal adhesions, and so these junctions were immunocytochemically imaged using IF microscopy (Figure S6) to gain a better understanding of the nature of the interactions of between hOBs with different substrates. The highest amount vinculin was

found along the extended actin microfilaments of cells seeded on NG TNTZ (Figure S8a), resulting in focal adhesion on the surface of these substrates.

Conclusions

In this study, the HPT process enabled us to control the grain size of a new type of alloy TNTZ to modulate both mechanical characteristics and wettability of substrates, which is highly dependent on the grain size and imperfections such as grain and subgrain boundaries and dislocations. High wettability of NG TNTZ substrates led to larger lamellipodia structures along with significantly higher numbers of filopodia protrusions all around the cells and hereby an excellent hOB cell attachment performance. Data regarding difference between cell projections with respect to different alloys observed in this study might lead to better understanding of cell – implant surface interaction for designing better implant materials. Furthermore, evidence of high level of vinculin expression and superior cell proliferation of hOB cells attached to NG TNTZ, suggests that an NG surface promotes cellular activity.

Acknowledgements

This work was performed in part on commission from the New Energy and Industrial Technology Development Organization (NEDO) and supported in part by Grants-in-Aid for Scientific Research (A), Young Scientists (A), Challenging Exploratory Research from the Japan Society for the Promotion of Science (JSPS), and Inter-University Cooperative Research Program “Innovation Research for Biosis-Abiosis Intelligent Interface” from the Ministry of Education, Culture, Sports, Science and Technology (MEXT), Japan. Authors kindly thank Dr. Xuetao Shi (Tohoku University, Japan) for providing the hOB cells used in this study.

References

1 P. K. C. Venkatsurya, B. Girase, R. D. K. Misra, T. C. Pesacreta, M. C. Somani and L. P. Karjalainen, *Mater. Sci. Eng. C*, 2012, **32**, 330–340.

2 A. Meyers, A. Mishra and J. Benson, *Prog. Mater. Sci.*, 2006, **51**, 427–556.

3 R. D. K. Misra, C. Nune, T. C. Pesacreta, M. C. Somani and L. P. Karjalainen, *Acta Biomater.*, 2013, **9**, 6245–58.

4 Y. Estrin, C. Kasper, S. Diederichs and R. Lapovok, *J. Biomed. Mater. Res. - Part A*, 2009, **90**, 1239–1242.

5 R. Z. Valiev, R. K. Islamgaliev and I. V Alexandrov, *Prog. Mater. Sci.*, 2000, **45**, 103–189.

6 R. Valiev, *Nat. Mater.*, 2004, **3**, 511–6.

7 A. Zhilyaev and T. Langdon, *Prog. Mater. Sci.*, 2008, **53**, 893–979.

8 M. Long and H. . Rack, *Biomaterials*, 1998, **19**, 1621–1639.

9 T. J. Webster and J. U. Ejiofor, *Biomaterials*, 2004, **25**, 4731–4739.

10 H. Yilmazer, M. Niinomi, M. Nakai, K. Cho, J. Hieda, Y. Todaka and T. Miyazaki, *Mater. Sci. Eng. C. Mater. Biol. Appl.*, 2013, **33**, 2499–507.

11 S. Faghihi, A. P. Zhilyaev, J. A. Szpunar, F. Azari, H. Vali and M. Tabrizian, *Adv. Mater.*, 2007, **19**, 1069–1073.

12 M. Niinomi, *Biomaterials*, 2003, **24**, 2673–2683.

13 R. Huiskes, H. Weinans and B. Van Rietbergen, in *Clinical Orthopaedics and Related Research*, 1992, pp. 124–134.

14 H. Yilmazer, M. Niinomi, K. Cho, M. Nakai, J. Hieda, S. Sato and Y. Todaka, *Acta Mater.*, 2014, **80**, 172–182.

15 A. A. Nazarov, A. E. Romanov and R. Z. Valiev, *Acta Metall. Mater.*, 1993, **41**, 1033–1040.

16 S. Shekhar, J. Cai, S. Basu, S. Abolghasem and M. R. Shankar, *J. Mater. Res.*, 2011, 26, 395–406.

17 M. B. Bever, D. L. Holt and A. L. Titchener, *Prog. Mater. Sci.*, 1973, **17**, 5–177.

18 T. Sakai, A. Belyakov, R. Kaibyshev, H. Miura and J. J. Jonas, *Prog. Mater. Sci.*, 2014, **60**, 130–207.

19 T. N. Kim, A. Balakrishnan, B. C. Lee, W. S. Kim, K. Smetana, J. K. Park and B. B. Panigrahi, *Biomed. Mater.*, 2007, **2**, S117–S120.

20 B. D. Boyan, T. W. Hummert, D. D. Dean and Z. Schwartz, *Biomaterials*, 1996, **17**, 137–146.

21 F. M. Fowkes, *Contact Angle, Wettability, and Adhesion*, American Chemical Society, Washington, D.C., 1964, vol. 43.

22 J. Wei, T. Igarashi, N. Okumori, T. Igarashi, T. Maetani, B. Liu and M. Yoshinari, *Biomed. Mater.*, 2009, **4**, 45002.

23 X. Shi, H. Chang, S. Chen, C. Lai, A. Khademhosseini and H. Wu, *Adv. Funct. Mater.*, 2012, **22**, 751–759.

24 K. Anselme, *Biomaterials*, 2000, **21**, 667–681.

25 S. Bindu, K. P. Sanosh, K. Smetana, a. Balakrishnan and T. N. Kim, *J. Mater. Sci. Technol.*, 2009, **25**, 556.

26 X. F. Walboomers, H. J. E. Croes, L. A. Ginsel and J. A. Jansen, *Biomaterials*, 1998, **19**, 1861–1868.

27 P. Hotulainen and P. Lappalainen, *J. Cell Biol.*, 2006, **173**, 383–94.

28 A. J. Ridley, M. A. Schwartz, K. Burridge, R. A. Firtel, M. H. Ginsberg, G. Borisy, J. T. Parsons and A. R. Horwitz, *Science*, 2003, **302**, 1704–1709.

29 J. Faix and K. Rottner, *Curr. Opin. Cell Biol.*, 2006, **18**, 18–25.

30 S. L. Gupton and F. B. Gertler, *Sci. STKE*, 2007, **2007**, re5.

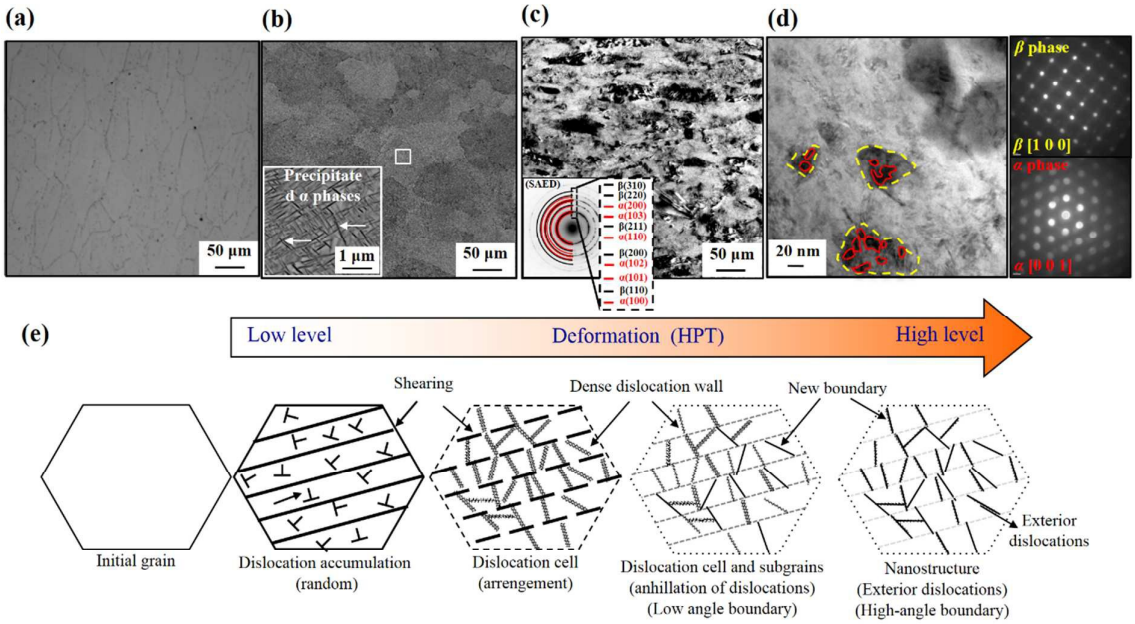

Figure 1 (a) Optical micrograph of $TNTZ_{ST}$ (b) SEM images of $TNTZ_{AT}$ (c) TEM bright image of $TNTZ_{AHPT}$ with selected area electron diffraction pattern (d) HRTEM bright field image with nano-beam diffraction patterns. (e) an illustration of dislocation generations and microstructural refinement mechanism. The precipitated α phases having needle-like morphology were shown with magnified SEM image. Precipitated α phases were marked with red line. The strain fields between β matrix and α phases were marked with yellow dashed line in the HRTEM image.

.

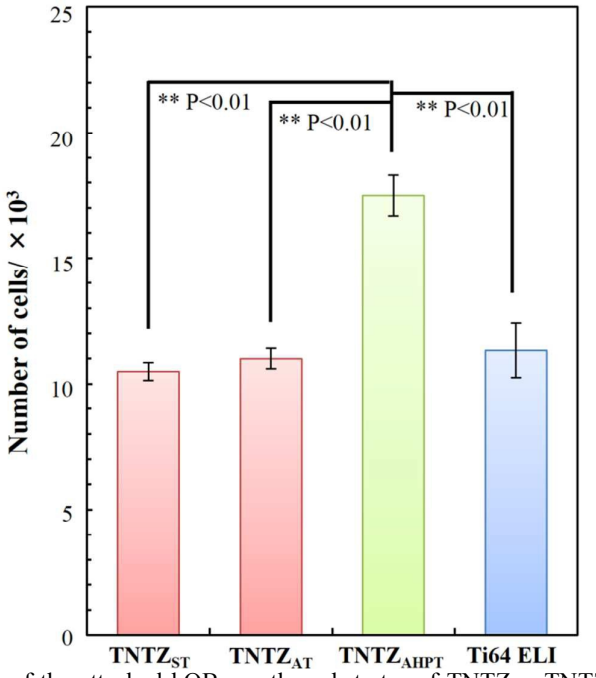

Figure 2 Average numbers of the attached hOBs on the substrates of $TNTZ_{ST}$, $TNTZ_{AT}$, $TNTZ_{AHPT}$, and Ti64 ELI after incubation for 6 h at 307K.

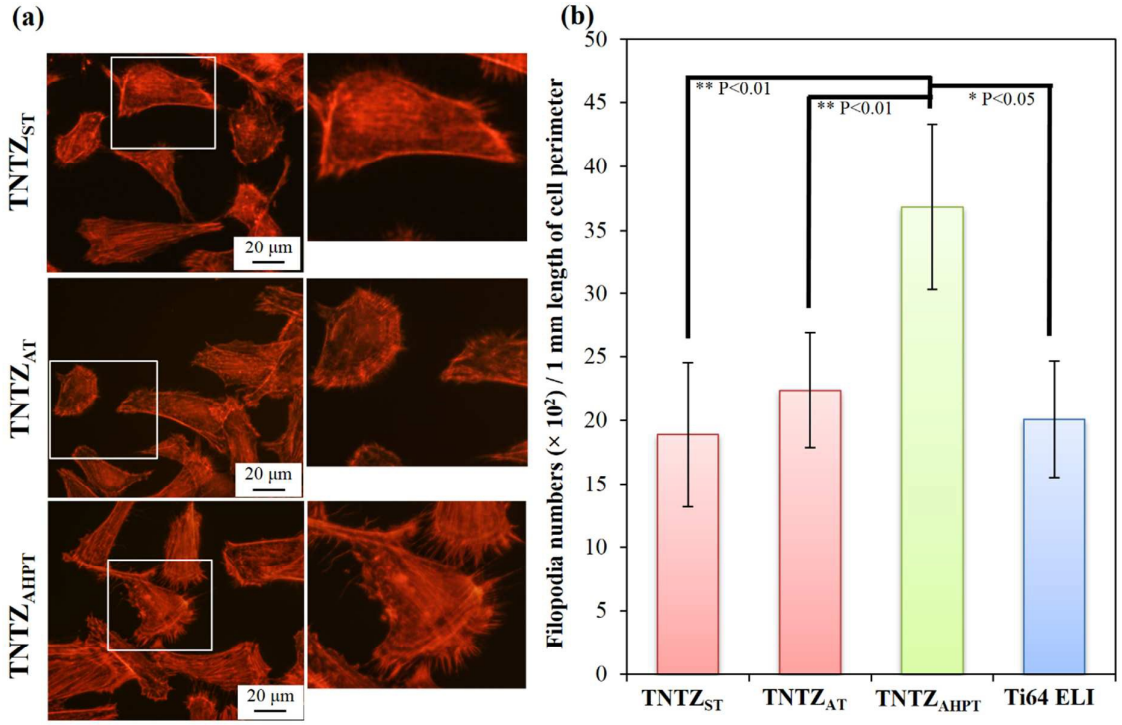

Figure 3. (a) Fluorescence micrographs of actin filaments and stress fibers, lamellipodia, and filopodia structures in hOBs attached on $TNTZ_{ST}$, $TNTZ_{AT}$, and $TNTZ_{AHPT}$ substrates and **(b)** number of filopodia spikes of hOBs attached on $TNTZ_{ST}$, $TNTZ_{AT}$, and $TNTZ_{AHPT}$, and Ti64 ELI substrates.